Journal of Photochemistry and Photobiology A: Chemistry 217 (2011) 76–86

Contents lists available at ScienceDirect

Journal of Photochemistry and Photobiology A: Chemistry

journal homepage: www.elsevier.com/locate/jphotochem

Spectroscopic properties of lanthanoid benzene carboxylates in the solid state: Part 2. Polar substituted benzoates

Matthias Hilder[a], Marina Lezhnina[b], Marcus L. Cole[a,1], Craig M. Forsyth[a], Peter C. Junk[a,*], Ulrich H. Kynast[b]

[a] School of Chemistry, Monash University, Clayton, Vic. 3800, Australia
[b] University of Applied Sciences Muenster, Dept. of Chemical Engineering, Applied Materials Sciences, Stegerwaldstr. 39, 48 565 Steinfurt, Germany

ARTICLE INFO

Article history:
Received 9 June 2010
Received in revised form
23 September 2010
Accepted 25 September 2010
Available online 25 October 2010

Keywords:
Europium
Terbium
Carboxylates
Luminescence

ABSTRACT

Europium and terbium complexes of *ortho*, *meta* and *para* substituted benzoate ligands including nitrobenzoate (NBA), aminobenzoate (ABA), hydroxybenzoate (OHBA) and methoxybenzoate (MeOBA) have been synthesised by metathesis reactions, carried out in aqueous media. The complexes were characterised by elemental, compositional and structural investigations, including microanalysis, EDTA titrations, differential thermal analysis, infra red spectroscopy, X-ray powder diffraction and single crystal structural analyses. Besides this, strong emphasis was on the determination of the optoelectronic properties of the compounds in the solid state. In this regard, reflectance, excitation and emission spectra were recorded. From these, the emission and excitation efficiencies were determined. The relative intensities as well as the splitting patterns of the $^5D_0 \rightarrow {}^7F_J$ transitions in the europium emission spectra are discussed.

1. Introduction

As noted in the first part [1] of this series, lanthanoids are widely used in various devices [2–12] due to their unique optoelectronic properties. Not only are they line emitters, the screened inner 4*f* electrons interact negligibly with the surrounding crystal field, hence their emission energies, and therefore colours, are of invariable energy [13–20].

To overcome the poor absorption properties [13,16,17,20–22] which are a limiting factor regarding luminescence performance, strongly absorbing ligands can be attached to the lanthanoid centre. These chromophores act as photon collectors, transferring the absorbed energy to the lanthanoid, thus exciting it indirectly. The metal can then relax to its electronic ground state accompanied by lanthanoid specific luminescence (antenna effect) [10,21]. Due to these properties, these compounds are also known as light converting molecular devices (LCMDs) [23].

Although the photophysical properties of many different classes of lanthanoid complexes have been studied [5,6,24–32], the individual results are often somewhat meaningless, since the light output is dependent on the experimental conditions (excitation wavelength, correction procedure) as well as sample preparation (solution, concentration, temperature). It was therefore decided to conduct a comprehensive study, characterising the complexes in their solid state, following a well documented measuring protocol.

This study focuses on europium (emits red light due to $^5D_0 \rightarrow {}^7F_2$ transition), gadolinium and terbium (emits green light due to $^5D_4 \rightarrow {}^7F_5$ transition) complexes of aromatic carboxylates. The carboxylate group strongly coordinates the highly oxophilic lanthanoids while the delocalised aromatic π electron system efficiently absorbs photons due $\pi^* \leftarrow \pi$ transitions. Gd compounds do not emit visible light. However, the phosphorescence spectra of the gadolinium complexes show signals resulting from triplet → singlet transitions and thus reflect the triplet state energies of the coordinated ligands.

The previous study [1] focussed on Eu^{3+} and Tb^{3+} complexes involving aromatic carboxylate ligands which were functionalised by hydrocarbon substituents. Therein we showed the effect conjugation had on the ligand to lanthanoid energy transfer efficiency and the emission efficiency, which were improved by the introduction of alkyl groups. In this study we now focus on benzoate ligands functionalised with polar substituents.

2. Results and discussion

2.1. Synthesis

The europium, gadolinium and terbium complexes were synthesised by aqueous metathesis reactions involving $EuCl_3/GdCl_3/$

* Corresponding author. Tel.: +61 03 9905 4570; fax: +61 03 9905 4597.
E-mail address: peter.junk@monash.edu (P.C. Junk).
[1] Present address: School of Chemistry, University of New South Wales, Sydney, NSW 2052, Australia.

1010-6030/$ – see front matter © 2010 Elsevier B.V. All rights reserved.
doi:10.1016/j.jphotochem.2010.09.021

$TbCl_3$ and slightly acidic sodium carboxylate solutions (pH 5–6) as reported previously [1] (see Eq. (1)). Following this procedure, europium, gadolinium and terbium complexes of *o*-, *m*-, *p*-nitrobenzoic acid (*o*-, *m*-, *p*-HNBA), *o*-, *m*-, *p*-aminobenzoic acid (*o*-, *m*-, *p*-HABA), *o*-, *m*-, *p*-hydroxobenzoic acid (*o*-, *m*-, *p*-HOHBA) and *o*-, *m*-, *p*-methoxybenzoic acid (*o*-, *m*-, *p*-HMeOBA) were synthesised. The ligands are presented in Fig. 1. In all reactions, a white precipitate of the lanthanoid tris-carboxylate deposited, except in the synthesis of europium *o*-hydroxobenzoate, a yellow precipitate was obtained. In the latter, by lowering the pH to three a white crystalline compound of different composition was formed. Both modifications are included in this study. The reaction yields ranged from 29% to 93% but were generally in the vicinity of 80%. The gadolinium complexes were synthesised solely to determine the triplet state energies of the ligands derived from phosphorescence measurements (see below).

$$LnCl_{3(aq)} + 3NaL_{(aq)} \rightarrow 3NaCl_{(aq)} + LnL_{3(s)} \quad (1)$$

(L = *o*-, *m*-, *p*-NBA; *o*-, *m*-, *p*-ABA; *o*-, *m*-, *p*-HBA; *o*-, *m*-, *p*-MeOBA. Levels of hydration not shown, see Section 4 for details)

2.2. Composition

The complexes were analysed using carbon microanalysis and EDTA complexometric methods. The compositions based on those results are presented in Table 1. The experimentally determined values are close to the experimentally expected ones (e.g. less than 1% discrepancy). Some compounds such as the terbium nitrobenzoates, have slightly higher differences in the terbium contents but since these compounds were not photophysically active it was decided not to pursue the investigation of these complexes any further.

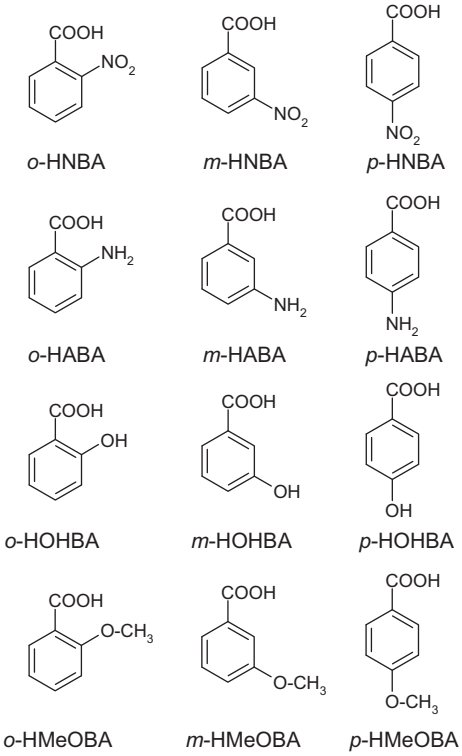

Fig. 1. Ligands used in this work.

2.3. Thermogravimetric analysis

Differential thermal analysis (TG/DTA) was used to analyse selected complexes. This investigation tool was applied only to

Table 1
Microanalytical data for all complexes.

Europium complexes			Terbium complexes		
Composition	Found	Calculated	Composition	Found	Calculated
Eu(*o*-NBA)$_3$(H$_2$O)$_2$	Eu = 21.7% C = 37.3%	Eu = 21.7% C = 36.7%	Tb(*o*-BA)$_3$(H$_2$O)$_2$	Tb = 22.9% C = 36.3%	Tb = 21.9% C = 36.4%
Eu(*m*-NBA)$_3$(H$_2$O)$_2$	Eu = 22.1% C = 36.5%	Eu = 21.7% C = 36.7%	Tb(*m*-NBA)$_3$(H$_2$O)$_2$	Tb = 23.4% C = 36.8%	Tb = 21.9% C = 36.4%
Eu(*p*-NBA)$_3$(H$_2$O)$_2$	Eu = 22.0% C = 37.1%	Eu = 21.7% C = 36.7%	Tb(*p*-NBA)$_3$(H$_2$O)$_2$	Tb = 23.0% C = 36.4%	Tb = 21.9% C = 36.4%
Eu(*o*-ABA)$_3$(H$_2$O)	Eu = 25.5% C = 44.4%	Eu = 26.3% C = 43.6%	Tb(*o*-ABA)$_3$(H$_2$O)	Tb = 27.2% C = 43.4%	Tb = 27.3% C = 43.1%
Eu(*m*-ABA)$_3$(H$_2$O)$_6$	Eu = 22.8% C = 38.6%	Eu = 22.7% C = 37.7%	Tb(*m*-ABA)$_3$(H$_2$O)$_6$	Tb = 23.9% C = 38.1%	Tb = 23.5% C = 37.3%
Eu(*p*-ABA)$_3$(H$_2$O)	Eu = 26.5% C = 43.4%	Eu = 26.3% C = 43.6%	Tb(*p*-ABA)$_3$(H$_2$O)	Tb = 27.2% C = 43.9%	Tb = 27.3% C = 43.1%
Eu(*o*-OHA)$_3$(H$_2$O)	Eu = 26.2% C = 43.3%	Eu = 26.1% C = 43.4%			
Eu(*o*-OHA)$_3$(H$_2$O)$_6$	Eu = 22.8% C = 38.3%	Eu = 22.6% C = 37.6%	Tb(*o*-OHBA)$_3$(H$_2$O)$_6$	Tb = 24.3% C = 38.0%	Tb = 23.4% C = 37.2%
Eu(*m*-OHBA)$_3$(H$_2$O)$_5$	Eu = 23.3% C = 38.0%	Eu = 23.2% C = 38.4%	Tb(*m*-OHBA)$_3$(H$_2$O)$_5$	 C = 37.3.6%	Tb = 23.4% C = 38.2%
Eu(*p*-OHBA)$_3$(H$_2$O)	Eu = 25.5% C = 42.3%	Eu = 26.0% C = 43.2%	Tb(*p*-OHBA)$_3$(H$_2$O)	Tb = 26.7% C = 43.0%	Tb = 27.0% C = 42.9%
Eu(*o*-MeOBA)$_3$(H$_2$O)$_4$	Eu = 23.1% C = 43.2%	Eu = 22.4% C = 42.6%	Tb(*o*-MeOBA)$_3$(H$_2$O)$_4$	Tb = 24.0% C = 43.0%	Tb = 23.2% C = 42.1%
Eu(*m*-MeOBA)$_3$(H$_2$O)$_2$	Eu = 24.3% C = 45.3%	Eu = 23.7% C = 44.9%	Tb(*m*-MeOBA)$_3$(H$_2$O)$_2$	Tb = 24.8% C = 44.7%	Tb = 24.5% C = 44.5%
Eu(*p*-MeOBA)$_3$	Eu = 24.4% C = 48.5%	Eu = 25.1% C = 47.6%	Tb(*p*-MeOBA)$_3$(H$_2$O)	Tb = 25.8% C = 46.9%	Tb = 26.0% C = 47.1%

Table 2
Weight loss determined by DTA.

Complex	Initial weight loss	Expected wt loss for nH_2O	Total weight loss (%)	Expected wt loss for oxide formation (%)
Tb(*o*-ABA)$_3$(H_2O)	3% (Exo: 115–180 °C)	3% (n = 1)	69	68
Eu(*p*-ABA)$_3$(H_2O)	3% (Exo: 120–220 °C)	3% (n = 1)	70	69
Eu(*o*-OHBA)$_3$(H_2O)	3% (Exo: 180–220 °C)	3% (n = 1)	70	70
Tb(*m*-OHBA)$_3$(H_2O)$_5$	14% (Exo: 100–280 °C)	14% (n = 5)	70	72

selected complexes to gain further evidence, and confidence of the compositions listed in Table 1. The results were in agreement with the previous volumetric and microanalytical data and confirm the suggested compositions of the synthesised complexes (Table 2).

2.4. IR data

ATR-FTIR spectra of the complexes were recorded and compared with the spectra of the free ligands. The stretching frequencies for the carbonyl groups (free acid) and the two carboxylate groups (complex) are presented in Table 3 (note that the aminobenzoic acid ligands exist as zwitter ions).

Following the classification described in the previous paper [1,33,34], the energy difference between the asymmetric and symmetric carboxylate stretching frequencies $\Delta\nu$ can be linked to structural features predominantly present in carboxylate complexes. Very small $\Delta\nu$ values (*e.g.* <100 cm^{-1}) are only observed for the *o*-nitrobenzoate complexes, suggesting very asymmetric carboxylate groups distorted by complex coordination modes.

The Eu(*o*-OHA)$_3$(H_2O) and Tb(*m*-OHBA)$_3$(H_2O)$_5$ complexes show very large $\Delta\nu$ values (*e.g.* >150 cm^{-1}). This has been suggestive of the presence of unidentate coordination modes. The spectra of the remaining complexes have a moderate separation (*e.g.* 120–150 cm^{-1}). Values of 150 cm^{-1} are associated with ideal symmetric carboxylate groups (C_{2v}) resulting from bridging and chelating coordination modes. Distortion caused by uneven coordination, such as binding selectively to one carboxylate oxygen, usually leads to smaller $\Delta\nu$ values. It should be noted that these are guidelines only. This is particularly true for the high coordinate lanthanoid complexes that combine several binding modes within the same coordination sphere.

Table 3
Stretching frequencies of C=O and CO_2^- vibrations (cm^{-1}).

Composition	HL	Ln = Eu	Ln = Tb
Ln(*o*-NBA)$_3$(H_2O)$_2$	ν(C=O): 1670	$\nu_{asy}(CO_2^-)$: 1489 $\nu_{sy}(CO_2^-)$: 1417–1412 $\Delta\nu(CO_2^-)$: 72–77	$\nu_{asy}(CO_2^-)$: 1489 $\nu_{sy}(CO_2^-)$: 1422–1413 $\Delta\nu(CO_2^-)$: 67–78
Ln(*m*-NBA)$_3$(H_2O)$_2$	ν(C=O): 1684	$\nu_{asy}(CO_2^-)$: 1553 $\nu_{sy}(CO_2^-)$: 1403 $\Delta\nu(CO_2^-)$: 150	$\nu_{asy}(CO_2^-)$: 1551 $\nu_{sy}(CO_2^-)$: 1403 $\Delta\nu(CO_2^-)$: 148
Ln(*p*-NBA)$_3$(H_2O)$_2$	ν(C=O): 1681	$\nu_{asy}(CO_2^-)$: 1556 $\nu_{sy}(CO_2^-)$: 1414 $\Delta\nu(CO_2^-)$: 142	$\nu_{asy}(CO_2^-)$: 1557 $\nu_{sy}(CO_2^-)$: 1422 $\Delta\nu(CO_2^-)$: 135
Ln(*o*-ABA)$_3$(H_2O)	ν(C=O): 1652 $\nu_{asy}(CO_2^-)$: 1566 $\nu_{sy}(CO_2^-)$: 1409	$\nu_{asy}(CO_2^-)$: 1505 $\nu_{sy}(CO_2^-)$: 1390 $\Delta\nu(CO_2^-)$: 115	$\nu_{asy}(CO_2^-)$: 1508 $\nu_{sy}(CO_2^-)$: 1392 $\Delta\nu(CO_2^-)$: 116
Ln(*m*-ABA)$_3$(H_2O)$_6$	$\nu_{asy}(CO_2^-)$: 1546 $\nu_{sy}(CO_2^-)$: 1390	$\nu_{asy}(CO_2^-)$: 1529 $\nu_{sy}(CO_2^-)$: 1398 $\Delta\nu(CO_2^-)$: 131	$\nu_{asy}(CO_2^-)$: 1526 $\nu_{sy}(CO_2^-)$: 1396 $\Delta\nu(CO_2^-)$: 132
Ln(*p*-ABA)$_3$(H_2O)	ν(C=O): 1655 $\nu_{asy}(CO_2^-)$: 1571 $\nu_{sy}(CO_2^-)$: 1415	$\nu_{asy}(CO_2^-)$: 1500 $\nu_{sy}(CO_2^-)$: 1384 $\Delta\nu(CO_2^-)$: 116	$\nu_{asy}(CO_2^-)$: 1502 $\nu_{sy}(CO_2^-)$: 1390 $\Delta\nu(CO_2^-)$: 112
Ln(*o*-OHBA)$_3$(H_2O)	ν(C=O): 1648	$\nu_{asy}(CO_2^-)$: 1550–1545 $\nu_{sy}(CO_2^-)$: 1380 $\Delta\nu(CO_2^-)$: 165–170	NA
Ln(*o*-OHBA)$_3$(H_2O)$_6$	ν(C=O): 1648	$\nu_{asy}(CO_2^-)$: 1535 $\nu_{sy}(CO_2^-)$: 1397 $\Delta\nu(CO_2^-)$: 138	$\nu_{asy}(CO_2^-)$: 1535 $\nu_{sy}(CO_2^-)$: 1400 $\Delta\nu(CO_2^-)$: 135
Ln(*m*-OHBA)$_3$(H_2O)$_5$	ν(C=O): 1676	$\nu_{asy}(CO_2^-)$: 1537 $\nu_{sy}(CO_2^-)$: 1413 $\Delta\nu(CO_2^-)$: 124	$\nu_{asy}(CO_2^-)$: 1527 $\nu_{sy}(CO_2^-)$: 1364 $\Delta\nu(CO_2^-)$: 163
Ln(*p*-OHBA)$_3$(H_2O)	ν(C=O): 1667	$\nu_{asy}(CO_2^-)$: 1500 $\nu_{sy}(CO_2^-)$: 1404 $\Delta\nu(CO_2^-)$: 96	$\nu_{asy}(CO_2^-)$: 1516 + 1489 $\nu_{sy}(CO_2^-)$: 1371 $\Delta\nu(CO_2^-)$: 118 + 145
Ln(*o*-MeOBA)$_3$(H_2O)$_4$	ν(C=O): 1663	$\nu_{asy}(CO_2^-)$: 1535–1518 $\nu_{sy}(CO_2^-)$: 1390 $\Delta\nu(CO_2^-)$: 128–145	$\nu_{asy}(CO_2^-)$: 1533–1516 $\nu_{sy}(CO_2^-)$: 1389 $\Delta\nu(CO_2^-)$: 127–144
Ln(*m*-MeOBA)$_3$(H_2O)$_2$	ν(C=O): 1680	$\nu_{asy}(CO_2^-)$: 1527 $\nu_{sy}(CO_2^-)$: 1394 $\Delta\nu(CO_2^-)$: 133	$\nu_{asy}(CO_2^-)$: 1527 $\nu_{sy}(CO_2^-)$: 1394 $\Delta\nu(CO_2^-)$: 133
Ln(*p*-MeOBA)$_3$(H_2O)	ν(C=O): 1666	$\nu_{asy}(CO_2^-)$: 1495 $\nu_{sy}(CO_2^-)$: 1374 $\Delta\nu(CO_2^-)$: 121	$\nu_{asy}(CO_2^-)$: 1496 $\nu_{sy}(CO_2^-)$: 1374 $\Delta\nu(CO_2^-)$: 122

2.5. Phase and structural analysis

Powder X-ray diffraction experiments were conducted on the isolated Eu and Tb products. To determine whether the compounds were isostructural to other known analogues they were compared with powder patterns generated from published single crystal data. Single crystals were obtained for some complexes ($Tb(o\text{-}MeOBA)_3(H_2O)_4$, $Tb(m\text{-}MeOBA)_3(H_2O)_2$ and $Tb(p\text{-}MeOBA)_3$). In these cases the molecular structures were determined using single X-ray analysis.

In all cases except of the *o*-hydroxobenzoate, the diffraction patterns of the europium and terbium compounds were essentially identical suggesting that the corresponding complexes are isostructural.

Although no Eu or Tb complexes are known of *o*-NBA the powder pattern is similar to those generated from the compounds with composition $[Ln(o\text{-}NBA)_3(H_2O)_2]_n$ (Ln = La [35], Ho [36] and Sm [36], established by single crystal determination) indicating the Eu and Tb *o*-NBA complexes are isostructural to these compounds. Although the powder patterns of the synthesised Eu and Tb *p*-NBA complexes match each other, the structure is different to the published single crystal X-ray structures of $[Ln_2(p\text{-}NBA)_6(H_2O)_4]_n$ (Ln = Eu [37], Tb [37,38]) as the generated powder patterns do not match.

The structures of the Eu and Tb *o*-ABA complexes are identical to $\{[Ln(o\text{-}ABA)_3(H_2O)_2](H_2O)\}_2$ (Ln = Er [39], Yb [39]). It should be mentioned that there are also two additional structural modifications namely $[La(o\text{-}ABA)_3]_n$ [39] and $[Nd(o\text{-}ABA)_3(H_2O)_3](H_2O)_3$ [39]. The structure of the present $Ln(m\text{-}ABA)_3(H_2O)_6$ (Ln = Eu, Tb) complexes is identical to the published structures of $[Ln(m\text{-}ABA)_3(H_2O)_3](H_2O)_3$ (Ln = Sm [40], Lu [41], Er [41] and Dy [40]), but is different to the Pr [42] or Nd [42] complexes, where the cation is significantly larger. The Eu and Tb *p*-ABA complexes are isostructural to the published single crystal X-ray structure of $[Tb(p\text{-}ABA)_3(H_2O)]_n$ [43].

Despite the fact that there are some published single crystal structures of europium and terbium *o*-hydroxobenzoates (Eu [44], Tb [45]), the two compounds with the composition of $Eu(o\text{-}HBA)_3(H_2O)_6$ and $Tb(o\text{-}HBA)_3(H_2O)_6$ are not the same. Interestingly the yellow Eu complex appears to be identical to the Gd structure of the $[Gd(o\text{-}OHBA)(H\text{-}o\text{-}OHBA)(o\text{-}OBA)(H_2O)]_n$ [46]. Eu and Tb *m*-hydroxobenzoate are isostructural to the published structures of $\{[Ln(m\text{-}OHBA)_3(H_2O)_3](H_2O)_2\}_n$ (Ln = Sm [47], Er [47], Nd [48]). No single structures of lanthanoid *p*-hydroxobenzoate complexes have been published.

Single crystals suitable for X-ray structural determination were obtained for the series of terbium *o*-, *m*- and *p*-methoxybenzoate complexes (Figs. 2–4, Tables 4–6). In all cases the bulk phase of the Tb and Eu analogues were identical with the single crystal phase as determined by comparison of the powder diffractogram generated from the single crystal data with data from X-ray powder diffraction.

The dimeric $\{[Tb(o\text{-}MeOBA)_3(H_2O)_2]\cdot(H_2O)_2\}_2$ complex crystallises in the triclinic space group *P-1*. The structure incorporates two symmetrical chelating bidentate ligands (Fig. 2). Every terbium has two water molecules coordinated to its centre. The third carboxylate ligand chelates to one centre and bridges to the second, resulting in a binuclear complex. Due to the tridentate nature, the carboxylate group is rather asymmetric, since the C–O distances for the two carboxylate groups are 1.246(5) Å (involving the monodentate oxygen atom), 1.279(5) Å (involving the bidentate oxygen atom) respectively and can be compared with the *symmetrical chelating* C–O bond lengths of 1.269(5) (C(1)–O(1)) and 1.271(5) (C(1)–O(2)) Å respectively. The overall coordination number of terbium is nine forming a doubled trigonal prism. The average Tb–O distance is 2.45 Å. The O–C–O angle range for the different carboxylate groups is fairly narrow, varying between 119.2° and 119.7°. The distance between the two Tb centres of the dimer is, with a value of 4.1 Å, fairly small. Hydrogen bonding between one of the coordinated water molecules and one of the oxygen atoms of the bidentate chelating carboxylate group leads to a three dimensional network. Additionally, the crystal lattice contains two free water molecules. The binuclear structure combines various carboxylate binding modes, resulting in a wide $\Delta\nu$ range, which is probably caused by complex coupling involving the various groups. The described structure is different to a published structure of Nd *o*-methoxybenzoate [49], meaning that there are structural variations of this ligand within the lanthanoid series.

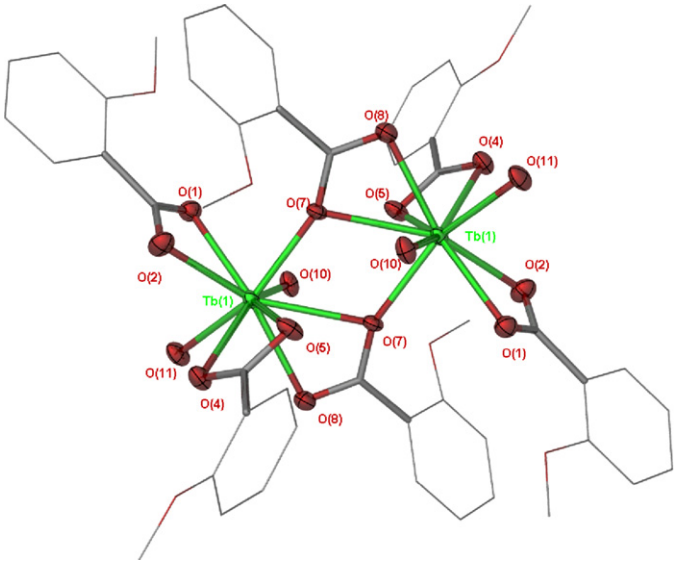

Fig. 2. X-ray crystal structure of $\{[Tb(o\text{-}MeOBA)_3(H_2O)_2]\cdot(H_2O)_2\}_2$.

The structure of terbium *m*-methoxybenzoate (Fig. 3) is identical to the structure of the published Eu analogue [50], which crystallizes in the monoclinic space group $P2_1/c$. The two dimensional chain structure of $[Tb(m\text{-}MeOBA)_3(H_2O)_2]_n$ only incorporates bidentate carboxylate groups, one being chelating while the other two are bridging. The chelating carboxylate group is involved in hydrogen bonding with water molecules of solvation. The coordination about the Tb^{3+} centre is completed by two water molecules,

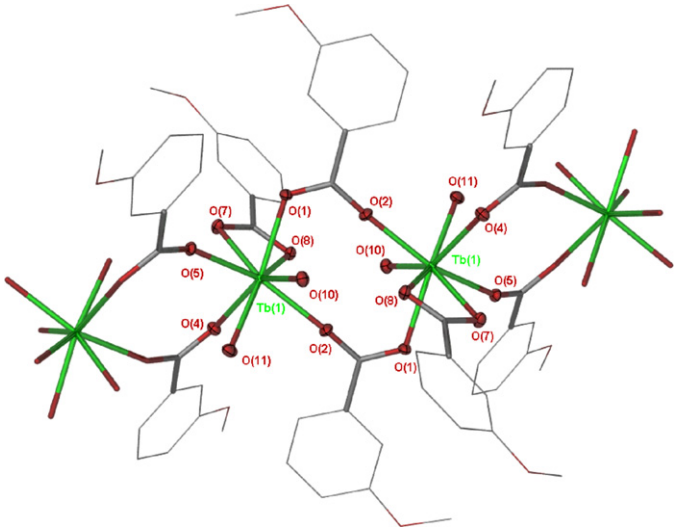

Fig. 3. X-ray crystal structure of $[Tb(m\text{-}MeOBA)_3(H_2O)_2]_n$.

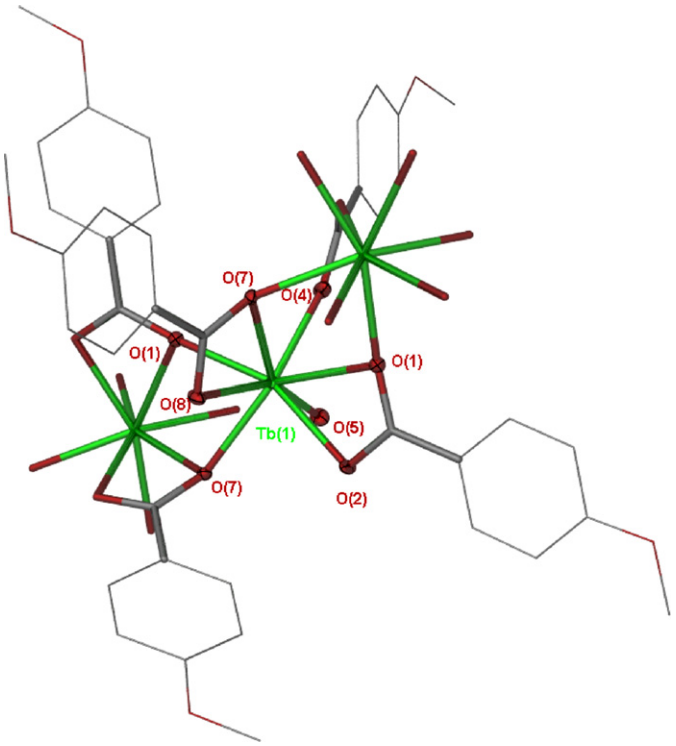

Fig. 4. X-ray crystal structure of $[Tb(p\text{-MeOBA})_3]_n$.

resulting in a coordination number of eight, forming a bicapped trigonal prism. The average Tb–O bond distance is 2.39 Å and the distance between two Tb centres is 5.2 Å into one direction and 4.6 Å in the other. The moderate $\Delta\nu$ values, which had been determined from the IR spectra, are in agreement with the observation that the carboxylate groups are reasonably symmetric.

$[Tb(p\text{-MeOBA})_3]_n$ crystallises in the monoclinic space group $P2_1/c$. The anhydrous complex forms a polymeric chain structure and incorporates terbium centres with eight coordinate dodecahedral geometry (Fig. 4). Every carboxylate is bridging, one is bidentate bridging, while the other two are tridentate chelating/bridging. Two Tb centres are connected by three bridging O–C–O groups. The average Tb–O bond length is 2.39 Å and the Tb–Tb distance is 3.9 Å. Again, the presence of slightly distorted carboxylate groups is indicated by the lower $\Delta\nu$ values.

Table 4
Bond lengths (Å) and angles (°) in $\{[Tb(o\text{-MeOBA})_3(H_2O)_2]\cdot(H_2O)_2\}_2$.

Selected bond distances	
Tb(1)–O(1)	2.381(2)
Tb(1)–O(2)	2.393(4)
Tb(1)–O(4)	2.355(2)
Tb(1)–O(5)	2.418(3)
Tb(1)–O(7)	2.463(2)
Tb(1)–O(7)#	2.357(3)
Tb(1)–O(8)	2.434(2)
Tb(1)–O(10)	2.453(2)
Tb(1)–O(11)	2.439(2)
Symmetry operator	
# $2-x, 1-y, 1-z$	
Selected bond angles	
O(1)–C(1)–O(2)	122.7(2)
O(4)–C(9)–O(5)	124.3(2)
O(7)–C(17)–O(8)	120.6(3)

Table 5
Bond lengths (Å) and angles (°) in $[Tb(m\text{-MeOBA})_3(H_2O)_2]_n$.

Selected bond distances	
Tb(1)–O(1)	2.513(3)
Tb(1)–O(2)	2.393(4)
Tb(1)–O(4)	2.484(3)
Tb(1)–O(5)	2.418(3)
Tb(1)–O(7)	2.610(3)
Tb(1)–O(8)	2.459(3)
Tb(1)–O(10)	2.422(3)
Tb(1)–O(11)	2.329(3)
Selected bond angles	
O(1)–C(1)–O(2)	119.3(4)
O(4)–C(9)–O(5)	119.6(4)
O(7)–C(17)–O(8)	119.7(4)

2.6. Absorption, excitation and emission properties

The photoelectronic properties of the complexes are summarised in Tables 7 and 8. For the lanthanoid emission to be efficiently sensitised, the triplet state of the ligand needs to be of sufficient energy. Additionally, it has to be higher than the emitting levels [8], which are the $^5D_0$ level for Eu^{3+} (17,000 cm^{-1}) and the $^5D_4$ level for Tb^{3+} (20,500 cm^{-1}) [10,13]. To prevent thermal or phonon assisted energy backtransfer, the energy levels should be separated by at least 207 cm^{-1} (*e.g.* thermal energy kT). Previous reports suggest that the triplet energies should be about 2500 cm^{-1} higher than these lanthanoid emission levels [51,52] to prevent thermal or phonon assisted energy backtransfer. At the same time, this value appears to grant sufficient overlap of triplet related states with the corresponding resonance levels. This is also in agreement with the findings in the first part of this series for typical excitation and emission spectra for $Ln(p\text{-MeC}_6H_4CO_2)_3]$ (Ln = Tb, Eu). [1] It should be noted that resonance and emissive levels do not necessarily have to be the same. Energy transfer from the ligand triplet is also conceivable into higher lanthanoid states (e.g. Eu^{3+} ($^5D_1$, $^5D_2$), or Tb^{3+} ($^5D_3$, $^5D_2$)), originating from which the usual phonon assisted relaxation into the emitting states, followed by emission can proceed. The hydroxybenzoic acids may serve as examples for this behaviour, (see Table 8).

In order to determine the triplet state energies for all the Eu^{3+} and Tb^{3+} complexes included in this study, we measured the phosphorescence spectra for the isostructural Gd^{3+} compounds of all ligands in this work (Table 8).

The absorption of neither complex containing nitro groups sensitises lanthanoid luminescence. This indicates that the energies of the triplet states must be very low, thus preventing efficient population of either of the resonance levels. The triplet state energies of

Table 6
Bond lengths (Å) and angles (°) in $[Tb(p\text{-MeOBA})_3]_n$.

Selected bond distances	
Tb(1)–O(1)	2.349(4)
Tb(1)–O(1)#	2.560(4)
Tb(1)–O(2)#	2.352(4)
Tb(1)–O(4)	2.284(4)
Tb(1)–O(4)#	2.508(4)
Tb(1)–O(5)#	2.303(4)
Tb(1)–O(7)	2.379(4)
Tb(1)–O(8)*	2.412(4)
Tb(1)–Tb(1)	3.919(1)
Symmetry operators	
#$x, 3/2-y, 1/2+z$	
*$x, 3/2-y, z-1/2$	
Selected bond angles	
O(1)–C(1)–O(2)	118.1(6)
O(4)–C(9)–O(5)	123.4(6)
O(7)–C(17)–O(8)	119.1(6)

Table 7
Absorption and emission properties of Eu and Tb carboxylate complexes.

Composition	Singlet–singlet absorption		Emission integral (excitation efficiency)	
	Eu	Tb	Eu	Tb
		300–400	No luminescence observed	No luminescence observed
Ln(*m*-NBA)$_3$(H$_2$O)$_2$	255–390	260–400	No luminescence observed	No luminescence observed
Ln(*p*-NBA)$_3$(H$_2$O)$_2$	250–350	265–400	No luminescence observed	No luminescence observed
Ln(*o*-ABA)$_3$(H$_2$O)	250–400	320–390	No luminescence observed	$\lambda_{ex=292\,nm}$: 3 498 112 (31)^L $\lambda_{ex=384\,nm}$: 6 102 323 (15)^p
Ln(*m*-ABA)$_3$(H$_2$O)$_6$	270–335	270–350	No luminescence observed	$\lambda_{ex=345\,nm}$: 7 755 418 (13)^p
Ln(*p*-ABA)$_3$(H$_2$O)	230–370	250–338	No luminescence observed	$\lambda_{ex=293\,nm}$: 8 800 642 (11)^L $\lambda_{ex=324\,nm}$: 8 754 580 (31)^p
Ln(*o*-OHBA)$_3$(H$_2$O)	265–400		No luminescence observed	
Ln(*o*-OHBA)$_3$(H$_2$O)$_6$	300–400	275–340	No luminescence observed	$\lambda_{ex=275\,nm}$: 7 325 754 (13)^L $\lambda_{ex=302\,nm}$: 7 378 217 (13)^p $\lambda_{ex=351\,nm}$: 6 747 003 (8)^p
Ln(*m*-OHBA)$_3$(H$_2$O)$_5$	300–400	260–340	No luminescence observed	$\lambda_{ex=290\,nm}$: 1 271 269 (18)^L $\lambda_{ex=380\,nm}$: 1 034 108 (29)^p
Ln(*p*-OHBA)$_3$(H$_2$O)	300–400	250–305	No luminescence observed	$\lambda_{ex=320\,nm}$: 2 049 346 (13)^L $\lambda_{ex=360\,nm}$: 680 276 (24)^p
Ln(*o*-MeOBA)$_3$(H$_2$O)$_4$	270–320	265–325	$\lambda_{ex=303\,nm}$: 606 543 (39)^L $\lambda_{ex=370\,nm}$: 317 689 (59)^p	$\lambda_{ex=300\,nm}$: 16 258 459 (16)^L $\lambda_{ex=335\,nm}$: 12 603 287 (15)^p
Ln(*m*-MeOBA)$_3$(H$_2$O)$_2$	270–310	270–325	$\lambda_{ex=292\,nm}$: 503 067 (51)^L $\lambda_{ex=320\,nm}$: 251 134 (47)^p $\lambda_{ex=368\,nm}$: 252 044 (62)^p	$\lambda_{ex=294\,nm}$: 9 355 010 (20)^L $\lambda_{ex=333\,nm}$: 8 247 456 (21)^p
Ln(*p*-MeOBA)$_3$(H$_2$O)	260–300	260–315	$\lambda_{ex=326\,nm}$: 165 584 (8)^L $\lambda_{ex=370\,nm}$: 211 523 (6)^p	$\lambda_{ex=294\,nm}$: 16 326 559 (18)^L $\lambda_{ex=360\,nm}$: 4 837 509 (18)^p

these complexes determined by phosphorescence measurements of the corresponding gadolinium compound, however, were well above 22,000 cm^{-1} (Table 8), which should, however weak, sensitise the emission of both lanthanoids. While the europium emission can be quenched by low energetic ligand to metal charge transfer, the energy difference for terbium might be too small to populate the high energy $^5D_4$ resonance level efficiently. As mentioned above, an energy separation of 2500 cm^{-1} seems to be favourable to result in intensive light emission. Additionally, the measurements were conducted at 77 K and temperature dependent structural changes might occur, which alter the triplet state energies. It is thus possible that the triplet state energy at room temperature is somewhat smaller than measured, preventing energy transfer to terbium altogether. Our results agree with other publications reporting that nitro derivatised benzoates are unable to sensitise lanthanoid emission [53]. However, de Bettencourt-Dias et al. reported examples of terbium and europium emission sensitised through nitrobenzoate ligands, for which triplet state energies of 25,020 to 25,620 cm^{-1} were determined [37]. This is counterintuitive since the samples also have a yellow tint, suggest electronic states extend into the visible. However, the data reported refer to solution species and are thus not instructive for the interpretation given here.

All other ligands sensitise Tb^{3+} emission indicating highly energetic triplet state energies of at least 2500 cm^{-1} above the emissive $^5D_4$ level. The intuitive assumption that triplet states of energy being sufficient enough to populate the high energetic resonance level of terbium must also be able to populate the lower energy resonance level of europium does not always hold. The fact that the complexes absorb UV light very strongly, but do not emit, suggests that the europium emission is quenched by low energetic ligand metal charge transfer states, changing the electron density of the ligand. These transitions are strong since they are quantum mechanically allowed and the low energy provides a non-radiative relaxation pathway for the excited states. The energies of those low energetic charge transfer states are increased for the methoxybenzoate ligands since both Eu^{3+} and Tb^{3+} emissions are observed here. The fact that the europium emission intensities are rather low indicates that the emission still seems to be affected by charge transfer states (the emission of the *ortho* and *meta* complexes is comparable to that of *o*-phenylbenzoate; the weak *para* complex emits like europium 1-naphthoate) [1]. From the two high emitters, europium *m*-MeOBA gets excited efficiently through the ligand while the *ortho* complex gets slightly more efficiently excited by direct $f \leftarrow f$ excitation. In the latter complex the energy levels are separated by 3000 cm^{-1} (from the Eu^{3+} $^5D_0$ level), which has previously shown to be beneficial for population. Nevertheless, the lower light output suggests that the *meta* complex is still affected by the interaction with CT states. Europium *p*-MeOBA seems to particularly suffer from this, therefore, even the advantageous energy separation of 3000 cm^{-1} regarding the Eu^{3+} $^5D_2$ level, cannot enable high emissivity, whereas the corresponding Tb^{3+} complex, in which the $^5D_4$ state serves as the resonance level, is one of the most efficient emitters. Previously, it has also been observed that high emission integrals only result from population of low energetic resonance levels ($^5D_0$) compared with higher ones ($^5D_2$). This agrees with earlier observations in this paper series in terms of energy separation and more intensive emission resulting from low energetic resonance levels [1].

Comparing the Tb emission, some are rather good emitters comparable to benzoates and dibenzoates (*m*/*p*-ABA, *o*-OHBA, *o*/*m*/*p*-MeOBA), while the remaining weaker ones are comparable to phenyl substituted benzoates [1]. The emission of the ABA complexes is similar for all three derivatives. Here the *ortho* complex is efficiently populated by the ligand (high excitation efficiency for ligand excitation), while for the others the energy separation is too large to be efficiently populated. The low emission integral of the *ortho* complex is therefore thought to be caused by dynamic quenching. Except for the strong *ortho* emitter, which does not seem to be affected by either static or dynamic quenching, the terbium OHBA complexes do not populate the terbium resonance levels efficiently. The levels separated by 3000 cm^{-1} are higher energy states ($^5D_1$), which might be possible for the low emission intensities. There is no significant difference in the excitation efficiencies (direct and ligand) for the strong MeOBA emitters. Here the *ortho* and *para* ligands have triplet states significantly higher than the $^5D_2$ level of europium, resulting in efficient population/emission. Surprisingly the triplet state of the *meta* complex has the same energy as the $^5D_4$ terbium level. This should lead to photon assisted energy back transfer, lowering the emission intensity.

Table 8
Triplet state energies ligands derived from phosphorescence measurements of the gadolinium complexes.

Gd^{3+} complex	E_T in cm^{-1}	ΔE in cm^{-1}	
o-NBA	22,272	5072 ($^5D_0$) 3222 ($^5D_1$) 722 ($^5D_2$)	1772 ($^5D_4$)
m-NBA	22,321	5121 ($^5D_0$) 3271 ($^5D_1$) 821 ($^5D_2$)	1821 ($^5D_4$)
p-NBA	22,321	5121 ($^5D_0$) 3271 ($^5D_1$) 821 ($^5D_2$)	1821 ($^5D_4$)
o-ABA	23,753	6553 ($^5D_0$) 4703 ($^5D_1$) 2253 ($^5D_2$)	3253 ($^5D_4$)
m-ABA	27,634	10,434 ($^5D_0$) 8584 ($^5D_1$) 6134 ($^5D_2$) 3234 ($^5D_3$) 2634 ($^5L_6$)	7134 ($^5D_4$) 1144 ($^5D_3$)
m-ABA	22,779	5579 ($^5D_0$) 3729 ($^5D_1$) 1279 ($^5D_2$)	2279($^5D_4$)
p-ABA	24,154	6954 ($^5D_0$) 5104 ($^5D_1$) 2654 ($^5D_2$)	3654($^5D_4$)
o-OHBA	27.027*	9827 ($^5D_0$) 7927 ($^5D_1$) 5527 ($^5D_2$) 2627 ($^5D_3$) 2027 ($^5L_6$)	6527 ($^5D_4$) 537 ($^5D_3$)
m-OHBA	29,940*	12,740 ($^5D_0$) 10,890 ($^5D_1$) 8440 ($^5D_2$) 5540 ($^5D_3$) 4940 ($^5L_6$) 2085 ($^5D_4$)	9440 ($^5D_4$) 3450 ($^5D_3$) 1968 ($^5L_9$) 1369 ($^5D_2$)
p-OHBA	29,851*	12,651 ($^5D_0$) 10,801 ($^5D_1$) 8351 ($^5D_2$) 5451 ($^5D_3$) 4851 ($^5L_6$) 1996 ($^5D_4$)	9351 ($^5D_4$) 3361 ($^5D_3$) 1879 ($^5L_9$) 1280 ($^5D_2$)
o-MeOBA	23,095*	5895 ($^5D_0$) 4045 ($^5D_1$) 1595 ($^5D_2$)	2595 ($^5D_4$)
m-MeOBA	20,492*	3292 ($^5D_0$) 1442 ($^5D_1$)	<0
p-MeOBA	24,876*	7676 ($^5D_0$) 5826 ($^5D_1$) 3376 ($^5D_2$) 476 ($^5D_3$)	4376 ($^5D_4$)

'*' indicates that spectra were recorded at room temperature while all others were recorded at 77 K.

Unless this is again structural cooling effect, this contradiction currently escapes our understanding. This would also explain why the emission integrals are somewhat lower compared with the other MeOBA complexes.

Reported triplet state energies for gadolinium *o*-OHBA (23,800 cm^{-1}), *p*-OHBA (23,530 cm^{-1}), *o*-ABA (25,230 cm^{-1}), *p*-ABA (24,445 cm^{-1}) and *o*-MeOBA (21,505 cm^{-1}) support the results presented in this paper [54].

2.7. Relaxation of selection rule due to J-mixing and crystal field coupling

Since the $^5D_0 \rightarrow {}^7F_1$ transition of the Eu^{3+} emission is a magnetic dipole transition ($\Delta J = 1$), its intensity remains unaffected by the electromagnetic environment and has therefore absolute character. By expressing the intensities of the other transitions relative to the intensity of the magnetically allowed $^5D_0 \rightarrow {}^7F_1$ transition it is possible to draw conclusions regarding electronic mechanisms, which are responsible for the gain in intensity [13–18]. The results are presented in Table 9.

The intensity of the strictly forbidden $^5D_0 \rightarrow {}^7F_0$ transition ($\Delta J = 0$) is relatively low for all complexes. This suggests that *J* mixing, the only possible mechanism relaxing this selection rule, is low.

All the relative intensities measured for the $^5D_0 \rightarrow {}^7F_2$ transitions, are exceptionally large. The intensities can be affected by *J* coupling as well as crystal field mixing. Since *J* coupling has widely been excluded based on the intensities of the $^5D_0 \rightarrow {}^7F_0$ transitions, the intensity must be caused mainly by crystal field effects, where the ligand mixes wavefunctions of even parity to the uneven parity of the 4*f* orbital, thus relaxing the parity selection rule. This statement is further supported by taking the $^5D_0 \rightarrow {}^7F_4$ transitions into account. Since the intensity is mainly affected by crystal field coupling, the intensities are related for the discussed complexes.

They intensity of the $^5D_0 \rightarrow {}^7F_3$ transition mainly reflects temporary distortion of the parity caused by vibration and is not of major importance for this discussion.

2.8. Crystal field analysis

The $^5D_0$ emission level of europium is non-degenerate and thus does not interact with the surrounding crystal field ($J = 0$). The splitting of the transition lines observed in the Eu^{3+} emission spectra is therefore solely caused by the *J* sublevels of the ^7F_J state. The splitting pattern can be used to determine the microsymmetry in regard to the europium centre [20]. The splitting for each transition is included in Table 9.

As mentioned above, the *o*-methoxybenzoate terbium complex consists of a doubled trigonal prism with D_{3h} symmetry. The theoretically expected splitting pattern for this configuration is observed for the $^5D_0 \rightarrow {}^7F_{0,1,2}$ transitions. Less components are observed for the lower energy emissions which reflects the lack of resolution of the low intensity transitions.

A splitting pattern of 1:3:4 for the $^5D_0 \rightarrow {}^7F_{0,1,2}$ transitions of the *m*-methoxybenzoate terbium complex is expected (bicapped trigonal prism: C_{2v}), which fits the measured emission spectrum rather well. Deviations are caused by a lack of resolution.

Also in good agreement is the splitting pattern of the *p*-methoxybenzoate terbium complex, where a dodecahedral environment with D_{2d} symmetry is formed around the europium centre. The expected splitting pattern for this configuration is 1:2:4 for the $^5D_0 \rightarrow {}^7F_{0,1,2}$ transitions.

Table 9
Relative intensities and line splitting of the $^5D_0 \rightarrow {}^7F_J$ transitions.

$^5D_0 \rightarrow {}^7F_J$ J=	Eu(*o*-MeOBA)$_3$(H_2O)$_4$	Eu(*m*-MeOBA)$_3$(H_2O)$_2$	Eu(*p*-MeOBA)$_3$(H_2O)
0	0.038 (1)	0.049 (1)	0.030 (1)
1	1.000 (2)	1.000 (2)	1.000 (2)
2	4.911 (3)	6.572 (4)	5.422 (4)
3	0.151 (2)	0.174 (1)	0.140 (1)
4	0.357 (3)	0.478 (2)	0.305 (3)

3. Conclusions

Various complexes of europium and terbium benzoates functionalised with polar substituents were synthesised following aqueous metathesis reaction routes. The compositions were determined by microanalysis, edta titrations and thermogravimetric analysis.

Dominant bonding features were concluded from IR measurements, which were in agreement with structural information from single crystal X-ray investigations. Most of the europium complexes were isostructural to their corresponding terbium analogues, which was evident from powder X-ray diffraction data. Additionally, some structures were identical to those previously published incorporating different lanthanoids. There are, however, two structural modifications for europium *o*-hydroxobenzoate. The structural phase was determined by powder XRD. Further structural conclusions were drawn from the IR spectra. The whole series of *ortho*, *meta* and *para*-methoxybenzoate complexes were structurally determined by single crystal X-ray crystallography.

Polar substituents lower the triplet state of the ligand, thus making it difficult to efficiently populate the low energetic $^5D_0$ state of Eu^{3+}. Nitrobenzoates do not sensitise europium or terbium luminescence. Additionally, the electromagnetic excitation energy shifts electron density from the electron rich ligands towards the lanthanoid centre (LMCT). This is effective for europium complexes since Eu^{3+} can be reduced to Eu^{2+} with relative ease. Combined with the low triplet states, ligand sensitised europium luminescence is not observed for nitrobenzoate, aminobenzoate and hydroxobenzoate complexes. This is not observed for methoxybenzoate complexes, which therefore seem to have LMCT states of appreciably higher energy. Those cases, which show ligand sensitised luminescence but low excitation efficiencies for ligand excitation, indicate inefficient population from the triplet state, i.e. an increased preference for radiationless deactivation of the triplets. Combined with low light outputs, the excited lanthanoid state may additionally be affected by dynamic quenching; low efficiencies for direct $f \leftarrow f$ excitation thus indicating excited lanthanoid states involved in dynamic quenching, whereas high $f \leftarrow f$ excitation efficiencies suggest that these complexes are less affected by dynamic quenching.

By comparing the intensities of the Eu^{3+} $^5D_0 \rightarrow {}^7F_J$ transitions relative to the absolute $^5D_0 \rightarrow {}^7F_1$ magnetic dipole transition, conclusions regarding effective J coupling and crystal field splitting could be derived. Furthermore, the splitting pattern of the $^5D_0 \rightarrow {}^7F_J$ transitions observed in the europium emission spectra could be used to determine the microsymmetry about the lanthanoid centre. Despite the spectral resolution (room temperature measurements) the findings were in close agreement with the coordination polyhedra found in the single crystal X-ray structures.

4. Experimental

4.1. General procedures

The europium and terbium contents were determined by complexometric EDTA titrations. Carbon contents were determined by a Carbon Sulphur Determinator ELTRA CS800. The combustion was carried out in the presence of tungsten and iron and the reaction took place in an oxygen stream. The instrument was calibrated using $BaCO_3$. The IR spectra were recorded in the range of 4000–650 cm^{-1} using a Perkin-Elmer Spektrum ATR spectrometer. DTA measurements were carried out in air, using a Netzsch STA 409 instrument, using aluminium oxide as a reference. The heat rate was 20 °C per minute and the weight and heat changes were determined in the range of 20–1000 °C. For phase analysis on the microcrystalline powders a Philips PW1130 equipped with a copper cathode ray tube PW2213/20 (60 kV, 1500 W), which generated CuK_α radiation was used. A 2θ range of 5–50° was scanned. If available the recorded diffractograms were compared with those calculated from published single crystal structures computed on the data contained in the CCDC database using the program Lazy Pulverex. Photophysical properties of the complexes were determined using an ARC photospectrometer, which was equipped with a xenon discharge lamp (excitation source) and a photomultiplier (detection unit). The excitation and emission monochromators could be operated synchronised (reflectance spectra) or independently from each other (excitation and reflectance spectra). The powder surface of the sample was irradiated with monochromatic light of the range between 250 and 400 nm. The intensity of the light reflected from the surface was detected by the photomultiplier, which was set to a sensitivity of 250 mV. No filters were used and the slit widths of both monochromators were set to 2 μm. Low wavelength sensitive gratings were used. Data were recorded in 1 nm intervals and doing three readings per point. The integration time was 500 ms. To eliminate wavelength dependent fluctuations in the lamp intensity and photomultiplier sensitivity as well as instrumental setup parameters, a white standard (CaF_2), was measured under the same conditions. The sample data was divided by the data of the white standard in order to obtain the real reflectance spectrum of the sample. The emission monochromator was set to the characteristic emission wavelength of the individual lanthanoid ion (612 nm for Eu^{3+}, 545 nm for Tb^{3+}), whereas the excitation monochromator excited the sample with monochromatic light in the range of 250–400 nm. A long wavelength sensitive grating was used for the emission monochromator set to a slit width of 0.25 μm and equipped with a 350 nm cut-off filter, whereas for the excitation monochromator, set to a slit width of 2 μm and equipped with a UG5 filter, a short wavelength sensitive grating was used. Using a photomultiplier sensitivity of 600 mV, data points were recorded in 1 nm intervals (three readings per point) and using an integration time of 500 ms. The excitation monochromator scanned the wavelength region between 250 and 400 nm. The excitation intensities were corrected by the multiplication of the wavelength dependent correction factor k. This was determined by characterising the standard phosphor BAM ($BaMgAl_{10}O_{17}:Eu^{2+}$) under the same conditions using the emission wavelength of 450 nm. Since the measured spectrum differs from the real BAM spectrum by a correction factor, this wavelength dependent factor k can be determined by dividing the intensities of the real BAM spectrum by the one measured with the instrument. The latter were provided by the Philips research laboratories in Aachen (Germany).

To characterise the emission properties of the complexes, the instrument parameters regarding the filters, grating and slit widths were the same used to record the excitation spectra. However, the excitation monochromator was set to the wavelength of maximum excitation intensity, obtained from the excitation spectrum. The emission monochromator scanned the region between 400 and 700 nm in 0.25 nm steps (three readings per point). Additionally the photomultiplier sensitivity was set to 1000 ms. To quantify the light output, the emission intensities were integrated over the visible region. In order to eliminate influences resulting from the intensity of the xenon discharge excitation lamp, the emission integral was multiplied by the correction factor k, which was dependent on the excitation wavelength and which has been determined before from the excitation spectrum. To obtain information about the photophysical pathway, the integrals were also divided by the intensity of the excitation at the particular excitation wavelength, which was also obtained from the excitation spectrum. In the case of the europium complexes the intensities of the $^5D_0 \rightarrow {}^7F_0$ (578–582 nm), $^5D_0 \rightarrow {}^7F_2$ (605–635 nm), $^5D_0 \rightarrow {}^7F_3$ (640–665 nm) and $^5D_0 \rightarrow {}^7F_4$ (675–705 nm) transitions were integrated sepa-

rately and the integral was given relative to the intensity of the magnetic allowed $^5D_0 \rightarrow {}^7F_1$ (582–605 nm) transition in order to draw conclusions about crystal field and *J*-mixing effects.

4.2. General synthetic procedure

Europium and gadolinium chloride solutions were made by dissolving Eu_2O_3 or Gd_2O_3 in hot hydrochloric acid until completely dissolved and were then diluted with distilled water to concentrations of ca. 0.5 mol/dm^3. To obtain a terbium chloride solution, Tb_4O_7 was dissolved in concentrated nitric acid. By adding an excess of sodium carbonate solution, terbium carbonate precipitated and was washed with water until the filtrate showed a neutral pH. Terbium carbonate was then dissolved in hydrochloric acid and then continued as described for the europium solution. Both solutions were analysed by EDTA titrations (c_{EDTA} = 0.01 mol/dm^3), which in turn was calibrated using a Zn^{2+} standard solution.

Approximately 0.5 g of carboxylic acid ligand was suspended in water and sodium carbonate solution was added until a pH of around five was reached and all insoluble acid was quantitatively converted into the soluble sodium salt. To this, the europium, gadolinium or terbium chloride solution was added with a molar ratio lanthanoid:ligand of 1:3. A precipitate of the corresponding lanthanoid carboxylate complex was formed. The pH was again adjusted to five and the reaction mixtures were stirred overnight to ensure completeness of the reaction. The suspensions were filtered and washed with ethanol and water. The products were then dried at room temperature to constant mass and then subjected to further investigations.

The gadolinium complexes were synthesized for comparison purposes only and are not an object of this study. Gd titrations and IR spectra of the Gd compounds were compared to those of the analogous europium and terbium complexes to ensure the complexes were of the same composition. No further structural investigation was conducted on the gadolinium compounds.

4.3. Physical data

Eu(o-NBA)$_3$(H$_2$O)$_2$
V_{Eu}: 1.99 cm^3 (0.52 mol/dm^3) = 1.04 mmol
$m_{H\text{-}o\text{-}NBA}$: 0.52 g = 3.11 mmol
$m_{product}$: 0.38 g (yield = 53.3%)

Tb(o-NBA)$_3$(H$_2$O)$_2$
V_{Tb}: 1.79 cm^3 (0.58 mol/dm^3) = 1.04 mmol
$m_{H\text{-}o\text{-}NBA}$: 0.52 g = 3.11 mmol
$m_{product}$: 0.21 g (yield = 29.2%)

Gd(o-NBA)$_3$(H$_2$O)$_2$
V_{Gd}: 2.00 cm^3 (0.50 mol/dm^3) = 1.00 mmol
$m_{H\text{-}o\text{-}NBA}$: 0.50 g = 3.00 mmol

Eu(m-NBA)$_3$(H$_2$O)$_2$
V_{Eu}: 2.11 cm^3 (0.52 mol/dm^3) = 1.10 mmol
$m_{H\text{-}m\text{-}BBA}$: 0.55 g = 3.29 mmol
$m_{product}$: 0.60 g (yield = 79.7%)

Tb(m-NBA)$_3$(H$_2$O)$_2$
V_{Tb}: 1.79 cm^3 (0.58 mol/dm^3) = 1.04 mmol
$m_{H\text{-}m\text{-}NBA}$: 0.52 g = 3.31 mmol
$m_{product}$: 0.53 g (yield = 73.7%)

Gd(m-NBA)$_3$(H$_2$O)$_2$
V_{Gd}: 2.00 cm^3 (0.50 mol/dm^3) = 1.00 mmol
$m_{H\text{-}m\text{-}NBA}$: 0.50 g = 3.00 mmol

Eu(p-NBA)$_3$(H$_2$O)$_2$
V_{Eu}: 2.15 cm^3 (0.52 mol/dm^3) = 1.12 mmol
$m_{H\text{-}p\text{-}NBA}$: 0.56 g = 3.35 mmol
$m_{product}$: 0.52 g (yield = 67.8%)

Tb(p-NBA)$_3$(H$_2$O)$_2$
V_{Tb}: 1.78 cm^3 (0.58 mol/dm^3) = 1.04 mmol
$m_{H\text{-}p\text{-}NBA}$: 0.52 g = 3.11 mmol
$m_{product}$: 0.36 g (yield = 50.1%)

Gd(p-NBA)$_3$(H$_2$O)$_2$
V_{Gd}: 2.00 cm^3 (0.50 mol/dm^3) = 1.00 mmol
$m_{H\text{-}p\text{-}NBA}$: 0.50 g = 3.00 mmol

Eu(o-ABA)$_3$(H$_2$O)
V_{Eu}: 2.62 cm^3 (0.52 mol/dm^3) = 1.36 mmol
$m_{H\text{-}o\text{-}ABA}$: 0.56 g = 4.08 mmol
$m_{product}$: 0.34 g (yield = 43.2%)

Tb(o-ABA)$_3$(H$_2$O)
V_{Tb}: 2.43 cm^3 (0.58 mol/dm^3) = 1.41 mmol
$m_{H\text{-}o\text{-}ABA}$: 0.58 g = 4.23 mmol
$m_{product}$: 0.59 g (yield = 71.5%)

Gd(o-ABA)$_3$(H$_2$O)
V_{Gd}: 2.43 cm^3 (0.50 mol/dm^3) = 1.22 mmol
$m_{H\text{-}o\text{-}ABA}$: 0.50 g = 3.65 mmol

Eu(m-ABA)$_3$(H$_2$O)$_6$
V_{Eu}: 2.48 cm^3 (0.52 mol/dm^3) = 1.29 mmol
$m_{H\text{-}m\text{-}ABA}$: 0.53 g = 3.87 mmol
$m_{product}$: 0.45 g (yield = 52.2%)

Tb(m-ABA)$_3$(H$_2$O)$_6$
V_{Tb}: 2.26 cm^3 (0.58 mol/dm^3) = 1.31 mmol
$m_{H\text{-}m\text{-}ABA}$: 0.54 g = 3.94 mmol
$m_{product}$: 0.33 g (yield = 37.2%)

Gd(m-ABA)$_3$(H$_2$O)$_6$
V_{Gd}: 2.43 cm^3 (0.50 mol/dm^3) = 1.22 mmol
$m_{H\text{-}m\text{-}ABA}$: 0.50 g = 3.65 mmol

Eu(p-ABA)$_3$(H$_2$O)
V_{Eu}: 2.43 cm^3 (0.52 mol/dm^3) = 1.26 mmol
$m_{H\text{-}p\text{-}ABA}$: 0.52 g = 3.79 mmol
$m_{product}$: 0.68 g (yield = 93.0%)

Tb(p-ABA)$_3$(H$_2$O)
V_{Tb}: 2.30 cm^3 (0.58 mol/dm^3) = 1.34 mmol
$m_{H\text{-}p\text{-}ABA}$: 0.55 g = 4.01 mmol
$m_{product}$: 0.72 g (yield = 92.0%)

Gd(p-ABA)$_3$(H$_2$O)
V_{Gd}: 2.43 cm^3 (0.50 mol/dm^3) = 1.22 mmol
$m_{H\text{-}p\text{-}ABA}$: 0.50 g = 3.65 mmol

Eu(o-OHBA)$_3$(H$_2$O)
V_{Eu}: 2.41 cm^3 (0.52 mol/dm^3) = 1.25 mmol
$m_{H\text{-}o\text{-}OHBA}$: 0.52 g = 3.77 mmol
$m_{product}$: 0.55 g (yield = 75.4%)

Eu(o-OHBA)$_3$(H$_2$O)$_6$
V_{Eu}: 2.27 cm^3 (0.52 mol/dm^3) = 1.18 mmol
$m_{H\text{-}o\text{-}OHBA}$: 0.63 g = 3.55 mmol
$m_{product}$: 0.34 g (yield = 79.5.2%)

Tb(o-OHBA)$_3$(H$_2$O)$_6$
V_{Tb}: 2.46 cm^3 (0.58 mol/dm^3) = 1.42 mmol
$m_{H\text{-}o\text{-}OHBA}$: 0.59 g = 4.27 mmol
$m_{product}$: 0.84 g (yield = 86.9%)

Gd(o-OHBA)$_3$(H$_2$O)$_6$
V_{Gd}: 2.41 cm^3 (0.50 mol/dm^3) = 1.21 mmol
$m_{H\text{-}o\text{-}OHBA}$: 0.50 g = 3.62 mmol

Eu(m-OHBA)$_3$(H$_2$O)$_5$
V_{Eu}: 2.32 cm^3 (0.52 mol/dm^3) = 1.21 mmol
$m_{H\text{-}m\text{-}OHBA}$: 0.50 g = 3.62 mmol
$m_{product}$: 0.52 g (yield = 65.0%)
Tb(m-OHBA)$_3$(H$_2$O)$_5$
V_{Tb}: 2.08 cm^3 (0.58 mol/dm^3) = 1.21 mmol
$m_{H\text{-}m\text{-}OHBA}$: 0.50 g = 3.62 mmol
$m_{product}$: 0.41 g (yield = 51.3%)

Gd(*m-OHBA*)$_3$(H_2O)$_5$
V_{Gd}: 2.41 cm^3 (0.50 mol/dm^3) = 1.21 mmol
$m_{H\text{-}m\text{-}OHBA}$: 0.50 g = 3.62 mmol

Eu(*p-OHBA*)$_3$(H_2O)
V_{Eu}: 2.32 cm^3 (0.52 mol/dm^3) = 1.21 mmol
$m_{H\text{-}p\text{-}OHBA}$: 0.50 g = 3.62 mmol
$m_{product}$: 0.60 g (yield = 84.7%)

Tb(*p-OHBA*)$_3$(H_2O)
V_{Tb}: 2.41 cm^3 (0.58 mol/dm^3) = 1.40 mmol
$m_{H\text{-}p\text{-}OHBA}$: 0.58 g = 4.20 mmol
$m_{product}$: 0.27 g (yield = 32.8%)

Gd(*p-OHBA*)$_3$(H_2O)
V_{Gd}: 2.41 cm^3 (0.50 mol/dm^3) = 1.21 mmol
$m_{H\text{-}p\text{-}OHBA}$: 0.50 g = 3.62 mmol

Eu(*o-MeOBA*)$_3$(H_2O)$_4$
V_{Eu}: 2.23 cm^3 (0.52 mol/dm^3) = 1.16 mmol
$m_{H\text{-}o\text{-}MeOBA}$: 0.53 g = 3.48 mmol
$m_{product}$: 0.22 g (yield = 29.0%)

Tb(*o-MeOBA*)$_3$(H_2O)$_4$
V_{Tb}: 2.16 cm^3 (0.58 mol/dm^3) = 1.25 mmol
$m_{H\text{-}o\text{-}MeOBA}$: 0.57 g = 3.75 mmol
$m_{product}$: 0.30 g (yield = 36.6%)

Gd(*o-MeOBA*)$_3$(H_2O)$_4$
V_{Gd}: 2.19 cm^3 (0.50 mol/dm^3) = 1.10 mmol
$m_{H\text{-}o\text{-}MeOBA}$: 0.50 g = 3.29 mmol

Eu(*m-MeOBA*)$_3$(H_2O)$_2$
V_{Eu}: 2.27 cm^3 (0.52 mol/dm^3) = 1.18 mmol
$m_{H\text{-}m\text{-}MeOBA}$: 0.54 g = 3.54 mmol
$m_{product}$: 0.27 g (yield = 35.1%)

Tb(*m-MeOBA*)$_3$(H_2O)$_2$
V_{Tb}: 2.02 cm^3 (0.58 mol/dm^3) = 1.17 mmol
$m_{H\text{-}m\text{-}MeOBA}$: 0.53 g = 3.51 mmol
$m_{product}$: 0.47 g (yield = 62.0%)

Gd(*m-MeOBA*)$_3$(H_2O)$_2$
V_{Gd}: 2.19 cm^3 (0.50 mol/dm^3) = 1.10 mmol
$m_{H\text{-}m\text{-}MeOBA}$: 0.50 g = 3.29 mmol

Eu(*p-MeOBA*)$_3$
V_{Eu}: 2.21 cm^3 (0.52 mol/dm^3) = 1.15 mmol
$m_{H\text{-}p\text{-}MeOBA}$: 0.52 g = 3.45 mmol
$m_{product}$: 0.62 g (yield = 88.6%)

Tb(*p-MeOBA*)$_3$
V_{Tb}: 1.95 cm^3 (0.58 mol/dm^3) = 1.13 mmol
$m_{H\text{-}p\text{-}MeOBA}$: 0.52 g = 3.39 mmol
$m_{product}$: 0.48 g (yield = 69.2%)

Gd(*p-MeOBA*)$_3$
V_{Gd}: 2.19 cm^3 (0.50 mol/dm^3) = 1.10 mmol
$m_{H\text{-}p\text{-}MeOBA}$: 0.50 g = 3.29 mmol

4.4. X-ray crystallography

Crystalline samples were mounted in viscous hydrocarbon oil on glass fibres. Crystal data were obtained using an Enraf-Nonius Kappa CCD diffractometer. X-ray data were processed using the DENZO program [55]. Structural solutions and refinements were carried out using SHELXL [56] with the graphical interface X-Seed [57]. All hydrogen atoms were placed in calculated positions using the riding model. Crystal data and refinement parameters are compiled below.

Crystallographic data (excluding structure factors) for the structures reported in this paper have been deposited with the Cambridge Crystallographic Data Centre as supplementary numbers CCDC 778619–778621. Copies of the data can be obtained free of charge on application to CCDC, 12 Union Road, Cambridge, CB2 1EZ, UK (fax: +44 (0) 1223 336033; e-mail: deposit@ccdc.cam.ac.uk).

Crystal data for *Tb*(*o-MeOBA*)$_3$(H_2O)$_4$: $C_{24}H_{29}O_{13}Tb$, M = 684.39, colourless prism, 0.30 × 0.05 × 0.05 mm^3, triclinic, space group *P*-1 (no. 2), a = 8.3760(17), b = 13.237(3), c = 13.809(3) Å, α = 61.84(3), β = 75.57(3), γ = 76.73(3)°, V = 1295.9(5) Å^3, Z = 2, D_c = 1.754 g/cm^3, F_{000} = 684, Nonius KAPPA CCD, MoKα radiation, λ = 0.71073 Å, T = 123(2) K, $2\theta_{max}$ = 55.0°, 12651 reflections collected, 5855 unique (R_{int} = 0.0467). Final *GooF* = 1.046, *R*1 = 0.0410, *wR*2 = 0.1037, *R* indices based on 5240 reflections with $I > 2$sigma(I) (refinement on F^2), 374 parameters, 12 restraints. Lp and absorption corrections applied, μ = 2.796 mm^{-1}.

Crystal data for *Tb*(*m-MeOBA*)$_3$(H_2O)$_2$: $C_{24}H_{25}O_{11}Tb$, M = 648.36, colourless prism, 0.10 × 0.10 × 0.10 mm^3, monoclinic, space group $P2_1/c$ (no. 14), a = 9.7090(19), b = 11.915(2), c = 21.337(4) Å, β = 95.54(3)°, V = 2456.8(8) Å^3, Z = 4, D_c = 1.753 g/cm^3, F_{000} = 1288, Nonius KAPPA CCD, MoKα radiation, λ = 0.71073 Å, T = 123(2) K, $2\theta_{max}$ = 55.0°, 19,213 reflections collected, 5630 unique (R_{int} = 0.0446). Final *GooF* = 0.994, *R*1 = 0.0254, *wR*2 = 0.0514, *R* indices based on 4443 reflections with $I > 2$sigma(I) (refinement on F^2), 344 parameters, 6 restraints. Lp and absorption corrections applied, μ = 2.939 mm^{-1}.

Crystal data for *Tb*(*p-MeOBA*)$_3$: $C_{24}H_{21}O_9Tb$, M = 612.33, colourless prism, 0.10 × 0.10 × 0.10 mm^3, monoclinic, space group $P2_1/c$ (no. 14), a = 13.383(3), b = 22.317(5), c = 7.6232(15) Å, β = 104.42(3)°, V = 2205.1(8) Å^3, Z = 4, D_c = 1.844 g/cm^3, F_{000} = 1208, Nonius KAPPA CCD, MoKα radiation, λ = 0.71073 Å, T = 123(2) K, $2\theta_{max}$ = 50.0°, 12,898 reflections collected, 3863 unique (R_{int} = 0.1093). Final *GooF* = 0.932, *R*1 = 0.0491, *wR*2 = 0.0662, *R* indices based on 2551 reflections with $I > 2$sigma(I) (refinement on F^2), 310 parameters, 48 restraints. Lp and absorption corrections applied, μ = 3.262 mm^{-1}.

Acknowledgements

We acknowledge the Australian Research Council for support. We also acknowledge an IPRS scholarship and Monash Graduate Scholarship (M.H.).

Appendix A. Supplementary data

Supplementary data associated with this article can be found, in the online version, at doi:10.1016/j.jphotochem.2010.09.021.

References

[1] M. Hilder, P. Junk, U. Kynast, M. Lezhnina, J. Photochem. Photobiol. A 202 (2009) 10–20.
[2] T. Steinkamp, F. Schweppe, B. Krebs, U. Karst, Analyst 128 (2003) 29–31.
[3] D. Kumar, K.G. Cho, Z. Chen, V. Craciun, P.H. Holloway, R.K. Singh, Phys. Rev. B 60 (1999) 13331–13334.
[4] J.M. De Souza, S. Alves, G.F. De Sa, W.M. De Azevedo, J. Alloys Compd. 344 (2002) 320–322.
[5] Z.Q. Gao, C.S. Lee, I. Bello, S.T. Lee, Synthetic Met. 111–112 (2000) 39–42.
[6] M. Guan, Z.Q. Bian, F.Y. Li, H. Xin, C.H. Huang, New J. Chem. 27 (2003) 1731–1734.
[7] S.H. Cho, S.H. Kwon, J.S. Yoo, C.W. Oh, J.D. Lee, K.J. Hong, S.J. Kwon, J. Electrochem. Soc. 147 (2000) 3143–3147.
[8] D. Parker, P.K. Senanayake, J.A.G. Williams, J. Chem. Soc. Perk. Trans. 2 10 (1998) 2129–2139.
[9] Y. Fukuda, H. Ohtaki, A. Tomita, S. Owaki, Radiat. Prot. Dosim. 65 (1996) 325–328.
[10] A. Beeby, S.W. Botchway, I.M. Clarkson, S. Faulkner, A.W. Parker, D. Parker, J.A.G. Williams, J. Photochem. Photobiol. B 57 (2000) 83–89.
[11] T. Justel, H. Bechtel, H. Nikol, C.R. Ronda, D.U. Wiechert, Proc. Electrochem. Soc. 98–24 (1999) 103–119.
[12] Y. Taguchi, H. Koda, K. Ogi, Photopolymer laminate and its use in signboard with long afterglow in dark (patent number 2002321316) Kokai Tokkyo Koho. 2002, (Toyobo Co., Ltd., Japan), p. 5.

[13] B.R. Judd, Atomic theory and optical spectroscopy, in: K.A. Gschneidner, L. Eyring (Eds.), Handbook on the Physics and Chemistry of the Rare Earths, North-Holland Publishing Company, 1988, p. 81.
[14] Z.B. Goldschmidt, Atomic properties free atom atomic theory and optical spectroscopy, in: K.A. Gschneidner, L. Eyring (Eds.), Handbook on the Physics and Chemistry of the Rare Earths, North-Holland Publishing Company, 1978, p. 1.
[15] P. Fulde, Crystal fields, atomic theory and optical spectroscopy, in: K.A. Gschneidner, L. Eyring (Eds.), Handbook on the Physics and Chemistry of the Rare Earths, North-Holland Publishing Company, 1979, p. 295.
[16] W.T. Carnall, The absorption and emission spectra of rare earth ions in solution, atomic theory and optical spectroscopy, in: K.A. Gschneidner, L. Eyring (Eds.), Handbook on the Physics and Chemistry of the Rare Earths, North-Holland Publishing Company, 1979, p. 171.
[17] C.A. Morrison, R.P. Leavitt, Spectroscopic properties of triplyionised lanthanides in transparent host crystals, atomic theory and optical spectroscopy, in: K.A. Gschneidner, L. Eyring (Eds.), Handbook on the Physics and Chemistry of the Rare Earths, North-Holland Publishing Company, 1982, p. 461.
[18] M. Dolg, H. Stoll, Electronic structure calculations for molecules containing lanthanoid atoms, atomic theory and optical spectroscopy, in: K.A. Gschneidner, L. Eyring (Eds.), Handbook on the Physics and Chemistry of the Rare Earths, Elsevier, 1996, p. 607.
[19] D. Garcia, M. Faucher, Crystal field in non-metallic (rare earth) compounds, atomic theory and optical spectroscopy, in: K.A. Gschneidner, L. Eyring (Eds.), Handbook on the Physics and Chemistry of the Rare Earths, Elsevier, 1995, p. 263.
[20] C. Görller-Walrand, K. Binnemans, Rationalization of crystal field parameterization, atomic theory and optical spectroscopy, in: K.A. Gschneidner, L. Eyring (Eds.), Handbook on the Physics and Chemistry of the Rare Earths, Elsevier, 1996, p. 121.
[21] D. Parker, Coord. Chem. Rev 205 (2000) 109–130.
[22] S. Shionoya, W.M. Yen, Phosphor Handbook, 1st ed., CRC Press, 1997.
[23] J.M. Lehn, Angew. Chem. Int. Ed. 29 (1990) 1304–1319.
[24] M.C.F.C. Felinto, C.S. Tomiyama, H.F. Brito, E.E.S. Teotonio, O.L. Malta, J. Solid State Chem. 171 (2003) 189–194.
[25] J. Dexpert-Ghys, C. Picard, A. Taurines, J. Inclusion Phenom. 39 (2001) 261–267.
[26] J.C.G. Buenzli, D. Wessner, Israel J. Chem. 24 (1984) 313–322.
[27] L.D. Carlos, M. Assuncao, L. Alcacer, Synthetic Met. 69 (1995) 587–588.
[28] M. Bredol, T. Justel, S. Gutzov, Opt. Mater. 18 (2001) 337–341.
[29] D. De Graaf, S.J. Stelwagen, H.T. Hintzen, G. De With, J. Non-Cryst. Solids 325 (2003) 29–33.
[30] H. Deng, D.L. Gin, in: 215th ACS National Meeting (Book of Abstracts) 1998, POLY-214.
[31] M. Bredol, U. Kynast, C. Ronda, T. Welker, Luminescent materials and methods for their preparation (patent number 4122009) 1993 (Philips Patentverwaltung G.m.b.H., Germany), 3.
[32] D. Sendor, P. Junk, U. Kynast, Solid State Phenom. 90–91 (2003) 521–526.
[33] R.C. Mehrotra, R. Bohra, Metal Carboxylates, 1st ed., Academic Press, 1983.
[34] G.B. Deacon, R.J. Phillips, Coord. Chem. Rev. 33 (1980) 227–250.
[35] J.-F. Ma, Z.-S. Jin, J.-Z. Ni, Jiegou Huaxue 15 (2) (1996) 85–92.
[36] J.-F. Ma, Z.-S. Jin, J.-Z. Ni, Chin. J. Struct. Chem. 13 (1994) 113.
[37] A. de Bettencourt-Dias, S. Viswanathan, Dalton Trans. (2006) 4093–4103.
[38] J.-F. Ma, Z.-S. Jin, J.-Z. Ni, Acta Crystallogr. C50 (7) (1994) 1008–1010.
[39] G.B. Deacon, M. Forsyth, P.C. Junk, S.G. Leary, G.J. Moxey, Polyhedron 25 (2006) 379–386.
[40] Y. Song, B. Yan, Z. Chen, J. Coord. Chem. 58 (2005) 647–652.
[41] A.E. Klimek, B. Klimek, K. Stepniak, Z. Rzaczynska, W. Brzyska, O.I. Bodak, L.G. Akselrud, V.V. Pavlyuk, V.A. Tafeenko, Z. Kristallogr. 200 (1992) 25–33.
[42] H. Flemig, Private Communication, 2006.
[43] H.-L. Sun, C.-H. Ye, X.-Y. Wang, J.-R. Li, S. Gao, K.-B. Yu, J. Mol. Struct. 702 (2004) 77–83.
[44] M. Yin, J. Sun, J. Alloy Compd. 381 (2004) 50–57.
[45] J.F. Ma, Z.S. Jin, J.Z. Ni, Jiegou, Huaxue, Chin. J. Struct. Chem. 10 (1991) 125–128.
[46] J.-P. Costes, J.-M. Clemente Juan, F. Dahan, F. Nicodeme, Dalton Trans. 7 (2003) 1272–1275.
[47] Y. Koizumi, H. Sawase, Y. Suzuki, T. Takeuchi, M. Shimoi, A. Ouchi, Bull. Chem. Soc. Jpn. 57 (1984) 1809–1817.
[48] A.E. Koziol, W. Brzyska, B. Klimek, A. Kula, G.J. Palenik, K. Stepniak, J. Coord. Chem. 21 (1990) 183–191.
[49] T.N. Polynova, B.B. Smolyar, T.F. Filippova, M.A. Porai-Koshits, S.B. Pirkes, Koord. Khim. 13 (1987) 130–135.
[50] X. Li, Q.-H. Jin, Y.-Q. Zou, K.-B. Yu, Z. Kristallogr, New Cryst. Struct. 216 (2001) 285–286.
[51] J. Reshmi, S. Biju, M. Reddy, Inorg. Chem. Commun. 10 (2007) 1091–1094.
[52] M. Ladva, H. Takalo, V.M. Mukkala, C. Matachescu, J.C. RodriguezUbis, J. Kankare, J. Luminescence 75 (1997) 149–169.
[53] B.S. Panigrahi, Spectrochim. Acta A 56 (7) (2000) 1337–1344.
[54] B. Yan, H. Zhang, S. Wang, J. Ni, J. Photochem. Photobiol. A 116 (3) (1998) 209–214.
[55] Z. Otwinowski, W. Minor, Methods Enzymol. 276 (1997) 307–326.
[56] G.M. Sheldrick, SHELXL-97, University of Göttingen, Germany, 1997.
[57] L.J. Barbour, J. Supramol. Chem. 1 (2001) 189–191.